Hindawi
Advances in Civil Engineering
Volume 2021, Article ID 4555802, 12 pages
https://doi.org/10.1155/2021/4555802

Research Article

Effects of GO/Al_2O_3 and Al_2O_3 Nanoparticles on Concrete Durability against High Temperature, Freeze-Thaw Cycles, and Acidic Environments

Mehdi Saliani,[1] **Amin Honarbakhsh**,[1,2] **Rahele Zhiani**,[3,4] **Seyed Mojtaba Movahedifar**,[1] **and Alireza Motavalizadehkakhky**[4,5]

[1]*Department of Civil Engineering, Neyshabur Branch, Islamic Azad University, Neyshabur, Iran*
[2]*New Materials Technology and Processing Research Center, Department of Civil Engineering, Neyshabur Branch, Islamic Azad University, Neyshabur, Iran*
[3]*New Materials Technology and Processing Research Center, Department of Chemistry, Neyshabur Branch, Islamic Azad University, Neyshabur, Iran*
[4]*Department of Chemistry, Neyshabur Branch, Islamic Azad University, Neyshabur, Iran*
[5]*Advanced Research Center for Chemistry, Biochemistry & Nanomaterial, Neyshabur Branch, Islamic Azad University, Neyshabur, Iran*

Correspondence should be addressed to Amin Honarbakhsh; amin_honarbakhsh@yahoo.com and Rahele Zhiani; r_zhiani2006@yahoo.com

Received 30 August 2021; Revised 1 November 2021; Accepted 25 November 2021; Published 13 December 2021

Academic Editor: Peng Zhang

Copyright © 2021 Mehdi Saliani et al. This is an open access article distributed under the Creative Commons Attribution License, which permits unrestricted use, distribution, and reproduction in any medium, provided the original work is properly cited.

In this paper, the effect of GO/Al_2O_3 and Al_2O_3 synthesized nanoparticles on the durability of concrete is studied. To this end, after the synthesis of nanoparticles and confirmation of nanoparticles fabrication by SEM and FT-IR spectra, three concrete samples for each experiment related to each mix design were prepared and subjected to freeze-thaw cycles, high temperature, and acidic environment. The results show that the samples containing GO/Al_2O_3 nanoparticles had the least weight loss in freeze-thaw cycles as well as better resistance against acidic environment and the lowest apparent changes at high temperature compared to the samples containing nano-Al_2O_3 and the samples without nanoparticles. The replacement of 2 wt.% of cement with GO/Al_2O_3 nanoparticles results in the highest increase in concrete durability. The presence of nanoparticles in the concrete microstructure and the validation of the results are investigated by FT-IR, SEM, and EDX spectra.

1. Introduction

Over the past few years, the durability of cement-based products has attracted the attention of researchers more than mechanical properties. In fact, an essential step in increasing the serviceability of different types of concrete structures is to improve their durability.

There is a strong desire for new materials to be introduced by designers, which can be a great alternative to traditional materials in producing more durable concrete. Nanomaterials are one of the most effective materials that have a great role in the durability of mortar and concrete. Currently, research on nanomaterials has attracted more attention. Such materials are used in building materials such as concrete to improve durability [1, 2]. Many researchers have combined the properties of concrete with nanomaterials [3, 4]. Recent results have shown that the addition of nanoparticles, including nano-SiO_2, nano-ZrO_2, nano-Fe_3O_4, nano-TiO_2, and nano-Al_2O_3, can lead to the reconstitution of the pore structure of concrete and effectively improve its mechanical properties and durability [5–8]. Nano-SiO2 added at the specified concentration not only increases the strength of the concrete but also acts as a cement replacement material [9].

Permeability is the most important concrete property and is strongly correlated with durability. Some species, such as chloride ions, SO_2, CO_2, and sulfates, are soluble in water, which in turn can penetrate the concrete. Other foreign forces can also damage concrete and other building materials, which severely impact the life of construction and building services, and it has been recognized as a global problem [10]. Many researchers have studied issues related to concrete permeability [11, 12]. Permeability is mainly determined by the microstructural properties of concrete such as pore size, microdevices, and joints. Therefore, the addition of additives and minerals (to modify the microstructure of the concrete) will lead to a good level of permeability [13, 14]. Nanoparticles do not appropriately mix in cement and agglomerate due to their high specific surface area. This problem can be solved by using powerful mixers. Another disadvantage of using nanoparticles in concrete is the possibility of their high water absorption, which can cause some problems in concrete. Using nanotechnology is increasing in developed countries. However, due to the high cost, it is not used in any regular structures [15].

The nanoparticles can also reduce the permeability of the concrete by the effect of nanofiller and pozzolanic reaction, especially the homogeneous surface transfer zone (ITZ), and reduce its porosity. It also has a favourable effect on increased frost resistance [16].

There have been few reports of the use of nano-Al_2O_3 in concrete, where the use of nano-alumina as a partial replacement by cement results in the formation of C-A-S (calcium aluminium silicate) gels in concrete [17]. Nano-alumina reacts with the calcium hydroxide produced by the hydration of calcium aluminates. Therefore, high purity nano-alumina can be added to improve the concrete properties [17].

Research results indicate that nano-alumina improves the mechanical properties of concrete, such as compressive and tensile strength, which also reduces water absorption and chloride penetration and improves the durability of concrete [18, 19].

Graphene oxide (GO) as a monolayer graphene derivative is derived from sp^2 hybrid carbon atoms by a mixture of carboxyl, hydroxyl, and epoxy properties [20]. Oxygen functional groups attached to the base plates and edges of the GO sheets modify the van der Waals interactions between the GO sheets and thereby improve its dispersion in water. Recent types of research have reported homogeneous dispersion of GO in cement matrices. GO also exhibits high values of tensile strength, dimension ratio, and large area [21]. One of the main problems of using graphene in concrete is the hydrophobicity of graphene particles and, as a result, their tendency to agglomerate. Various methods, such as using surfactants, have been used to solve this problem. Recent studies have shown that adding 1 wt.% GO can simultaneously improve the strength of GO-chitosan composites [22].

Li et al. reported that carboxylic acid groups can react with calcium silicate hydrate (C-S-H) to form strong covalent bonds while GO has been extensively studied in the field of polymer composites [23].

Ma and Zhu investigated the effect of nano-SiO_2 and basalt on the strength and microstructure of concrete. They used nano-SiO_2 in their study and found that the replacement of 1.2 wt.% of cement by nano-SiO_2 results in maximum production of C-S-H gel and consequently higher compressive strength of concrete [24].

Zhang et al. worked on the workability, fracture property, and compressive strength of fly ash (FA) and metakaolin (MK) based geopolymer/alkali-activated mortar modified with polyvinyl alcohol (PVA) fiber and nano-SiO_2. They found that PVA fiber increases fracture performance and compressive strength but reduces workability. The optimal value of PVA fiber was 0.8%–1%. Moreover, 1% adding nano-SiO_2 to the mortar results in a slight improvement in the mechanical properties and workability with any amount of fiber added to the mortar [25].

Wang et al. studied the effects of fly ash (FA) and phosphorous slag (PS) on C-S-H structure, long-term hydration heat, and volume deformation of cement-based materials. They found that the addition of 30 wt.% PS decreased the 180-day hydration heat and shrinkage by about 9.2% and 9%, respectively. Moreover, due to the reaction of PS with CH, lots of C-S-H were produced with a high polymerization degree. Comparing the effect of FA with PS, they claimed that FA is more effective in decreasing the long-term hydration heat, as well as shrinkage and increasing the polymerization and Al content of C-S-H [26].

The purpose of this paper is to synthesize and compare GO/Al_2O_3 and Al_2O_3 and nanoparticles to investigate the effect of nanoparticles on concrete durability against freeze-thaw cycle, acidic environment, and high heat. The results in concrete containing GO/Al_2O_3 and Al_2O_3 nanoparticles were compared with concrete without nanoparticles.

2. Materials and Methods

Chemical materials were purchased from Fluka and Merck in high purity. FT-IR spectra were recorded on a VERTEX 70 spectrometer (Bruker) in the transmission mode in spectroscopic grade KBr pellets for all the powders. The particle size and structure of nanoparticle were observed using a Philips CM10 transmission electron microscope operating at 100 kV. Powder X-ray diffraction data were obtained using the Bruker D8 Advance model with Cu ka radiation.

2.1. Synthesis of Nanocomposites

2.1.1. Preparation of Graphite Oxide from Graphite. A mixture of graphite powder (5 g), sodium nitrate (2.5 g), and concentrated sulfuric acid (115 ml) was put in a balloon in an ice water bath for 15 min. The temperature should be controlled all the time should not exceed 15 ˚C.

The mixture was stirred in the ice bath for two hours. Then, the bath temperature was raised to 35 ˚C and stirred for 30 minutes. Then, 230 ml of deionized water was added slowly. The resulting brown suspension was stirred for 15 minutes at 95–98 ˚C. It was then diluted with deionized water. Then, 30% (50 ml) hydrogen peroxide was added dropwise. After adding hydrogen peroxide, the suspension

begins to bubble. When the temperature reached 40 °C, the hot suspension was filtered off and washed with 5% hydrochloric acid and deionized water to remove excess acid. Subsequently, some deionized water was added to the oxide graphite and centrifuged. The resulting oxide graphite was dried in a vacuum oven at 60 °C for 12 h [27].

2.1.2. Preparation of Graphene Oxide (GO) Nanosheets from Graphite Oxide. 400 ml of deionized water was added to the 0.4 g graphite oxide prepared in the previous step and placed in an ultrasonic bath for one hour. The resulting sediment was isolated, and the graphene oxide plates were dried for 24 h after drying in a vacuum oven at 80 °C [27].

2.1.3. The Synthesis Method of GO/Al_2O_3 Nanoparticle. 20 mg of $AlCl_3.8H_2O$ and polyethylene glycol (0.2 g) were mixed in 20 ml deionized water for 1 h. 200 mg of GO powder was added to this mixture and stirred for 30 minutes using the ultrasonic method. The reaction was continued at 150 °C for 24 hours. After cooling in the medium, the resulting sediment was washed several times with ethanol and deionized water and then dried at a vacuum at 80 °C for 1 h.

2.2. Raw Materials and Consumable Materials in Experiments

2.2.1. Cement. Portland cement, Moderate Sulfate Resistant (Type II), is one of the products of the Eastern Cement Factory Complex. The reason for the use of type II cement in this research is its high use in industry, especially in urban projects. The products of the Eastern Cement Factory Complex are mainly of this type.

2.2.2. Aggregates. Two types of aggregates were employed. Crushed limestone aggregates from Neyshabur mines were used as the coarse aggregates (gravel), which passed through 19 mm sieve and river sand as the fine aggregates which passed through 4.75 mm sieve. Fine and coarse aggregates size distribution is shown in Figure 1, which is in accordance with the ASTM C33 standard [28].

2.2.3. Water. In this study, Neyshabur drinking water has been used. The values of sulfate, chloride, and pH of the solution are 17 mg/*l*, 25 mg/*l*, and 7, respectively.

2.2.4. Superplasticizer. The applied superplasticizer is a neutral superplasticizer, abbreviated as 102N, from Concrete Chemical Products. This liquid superplasticizer is dark brown in accordance with ASTMC1017 standards. According to the catalog of Concrete Chemical Company, the desired plasticizer is compatible with cement and microsilica.

2.3. Mix Design. The consumable materials in concrete mixtures and their proportions are as follows.

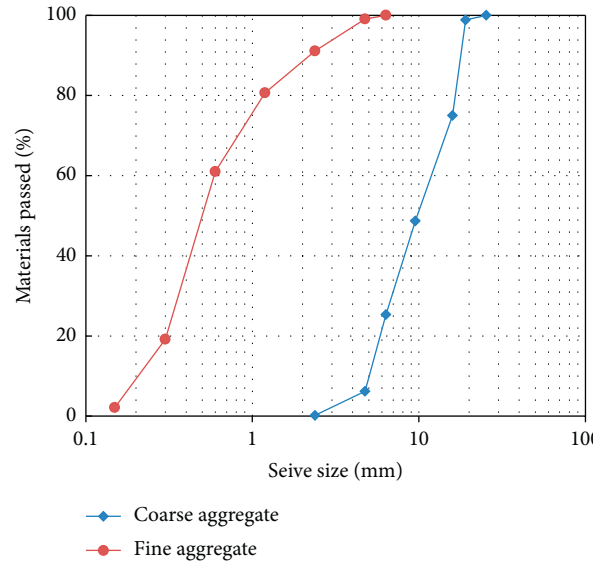

Figure 1: Fine and coarse aggregates size distribution.

2.3.1. Water-to-Cement Ratio. The water-to-cement ratio used in the samples prepared to obtain durable concrete is considered in accordance with the table provided in ACI318-83 [29]. Under the present conditions, the ratio of water to cement is 0.45.

2.3.2. Amount of Cement. The amount of cement consumed in laboratory samples is 325 $kg.m^{-3}$.

2.3.3. Superplasticizer. The proposed amount of superplasticizer was 1–4% of the cement content. In the mix design, polycarboxylate ether plasticizer was used, and adding superplasticizer was carried out until the slump of 10 cm was reached, which was about 2%.

2.3.4. Nanoparticles. The amount of Al_2O_3 and GO/Al_2O_3 used as an alternative to cement in concrete is 1% to 4% of the binder by weight.

Three cubic samples of 15 × 15 × 15 cm have been prepared in the laboratory for each experiment related to each mix design. Then, for each experiment of each mix design, three samples were examined and the average results of these three samples are considered. The mix designs of these samples are presented in Table 1.

In order to determine compressive strength, the cubic specimens were tested according to BS 1881: Part 116 Standard by Hydraulic Test Jack [30], as shown in Figure 2.

2.4. Concrete Tests

2.4.1. Freeze-Thaw Test. In this test, samples prepared according to ASTM C666 standard B are frozen inside the cooling system [31]. Then, they are immersed in warm water to go through the process of melting. For each day, 3 cycles of freeze and thaw were performed. After the number of test cycles is completed, the weight loss of the samples is measured.

Table 1: Required aggregates for the investigated mix design (kg.m^{-3}).

Specimen	Cement (kg/m^3)	Water (kg/m^3)	GO/Al_2O_3 (kg/m^3)	Al_2O_3 (kg/m^3)	Sand (kg/m^3)	Gravel (kg/m^3)	Superplasticizer (kg/m^3)
Control sample	400	180	—	—	1225	525	0.6
GO/Al_2O_3 1%	396	180	4	—	1225	525	0.6
GO/Al_2O_3 2%	392	180	8	—	1225	525	0.6
GO/Al_2O_3 3%	388	180	12	—	1225	525	0.6
GO/Al_2O_3 4%	384	180	16	—	1225	525	0.6
Al_2O_3 1%	396	180	—	4	1225	525	0.6
Al_2O_3 2%	392	180	—	8	1225	525	0.6
Al_2O_3 3%	388	180	—	12	1225	525	0.6
Al_2O_3 4%	384	180	—	16	1225	525	0.6

Figure 2: Hydraulic test Jack.

2.4.2. Acidic Environment. Sulfuric acid was added to water to reach pH 1.0 (1% concentration). All samples were weighed before immersion in sulfuric acid solution. Then, the mean weights of the samples were measured after acid exposure at 4, 8, 12, and 16 weeks according to ASTM C1012 [32]. Then, the compressive strength of the samples was examined.

2.4.3. High Temperature. The dried concrete samples were placed in the furnace at temperatures of 200 °C, 400 °C, and 600 °C for 4 hours, and the color changes and crack growth of the concrete samples are investigated [33].

3. Results

Two infrared spectroscopy and scanning electron microscopy analyzes were used to investigate the nanoparticles as follows.

3.1. Nanocomposite Analysis

3.1.1. Infrared Spectrum Analysis (FT-IR). The synthesized GO and GO/Al_2O_3 are characterized using FT-IR spectra (Figure 3). The prepared GO index band appeared at about 1725 cm^{-1}. Two prominent peaks of nanocomposites are observed at about 1400 and 1109 cm^{-1}. Figure 4(b) is a C–C tensile bond at 1392 cm^{-1}. The other peak, about 1119 cm^{-1}, corresponds to the Al–O–C bond. This bond implies that our process creates a chemical bond between the GO sheets and the alumina matrix [34].

3.1.2. Investigating the Formation of GO/Al_2O_3 (SEM). The structure of GO/Al_2O_3 nanoparticles was analyzed using SEM. The observations showed that the nanoparticles have uniform structures (Figure 5).

3.2. Concrete Durability Results

3.2.1. Freeze-Thaw Test. In this test, samples are prepared according to ASTM C666 standard B and are frozen inside the cooling system. Then, they are immersed in warm water to go through the process of melting. For each day, 3 cycles of freeze and thaw were performed. After the number of test cycles is completed, the weight loss of the samples is measured.

Figure 6 compares the weight loss of nano-GO/Al_2O_3 and nano-Al_2O_3 samples. In this figure, the effect of GO/Al_2O_3 nanoparticles on frost resistance is clearly evident. The amount of weight loss in GO/Al_2O_3 nanoparticles is lower than that of nono-Al_2O_3.

Moreover, the concrete samples containing nano-GO/Al_2O_3 and nano-Al_2O_3 are more durable against freeze-thaw cycles than those without nanoparticles.

The compressive strength under different freeze-thaw cycles is conducted, and the results are shown in Figure 7 for different contents of Al_2O_3 and GO/Al_2O_3 nanoparticles. As shown in Figure 7, at 300 freeze-thaw cycles, the sample containing 2% GO/Al_2O_3 nanoparticles has the highest compressive strength (33.7 MPa) and the lowest decrease in compressive strength, which is about 10.8%. Note that, at 300 freeze-thaw cycles, the compressive strengths of the control sample and the sample containing 2% Al_2O_3 nanoparticles are, respectively, 25.7 MPa and 31.8 MPa,

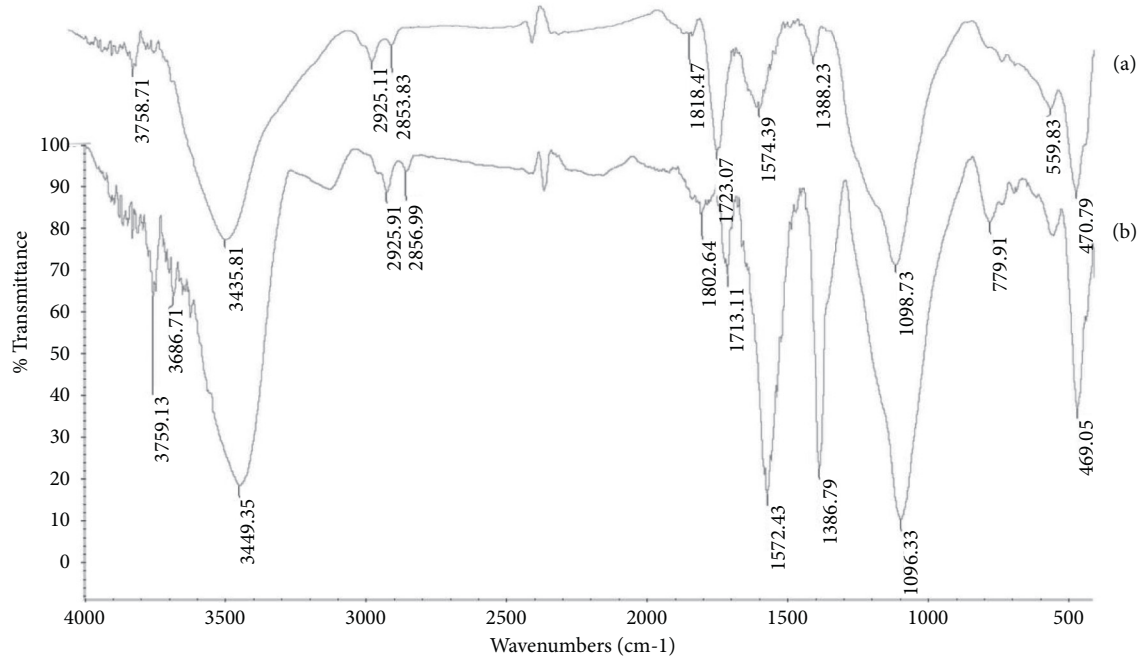

Figure 3: FT-IR spectra of GO (a) and GO/Al_2O_3. (b) Sharp peak in the 594 cm^{-1} region corresponds to Al–O, which confirms the synthesis of Al_2O_3 (Figure 4).

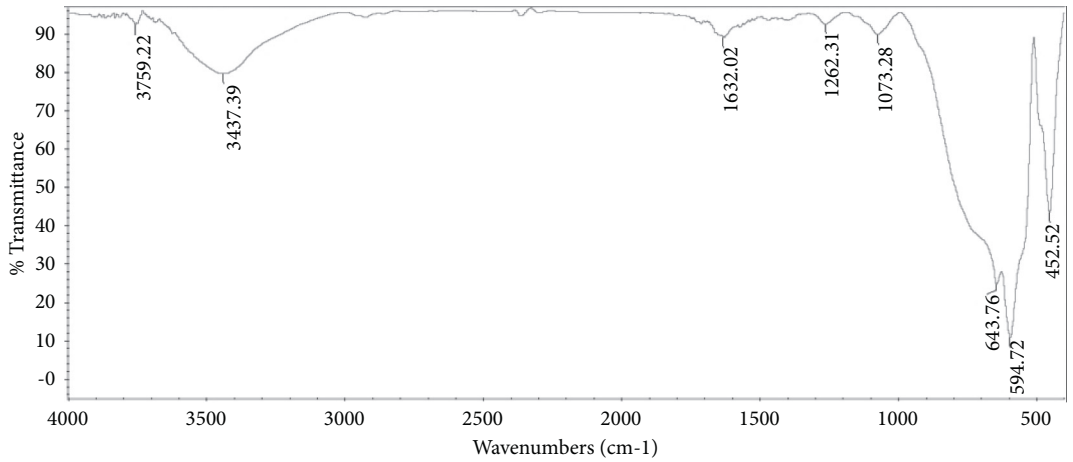

Figure 4: FT-IR spectrum of Al_2O_3.

which show 19.9% and 12.9% reduction in compressive strength.

3.2.2. Effects of High Temperature on the Appearance of Concrete. The effects of high temperature on the color changes and crack growth of the concrete samples are investigated. The samples do not experience any color change at 200 °C; however, they become yellowish with higher temperature and tend to be white at 600 °C. Moreover, as the temperature rises, the crack growth increases. Figure 8 shows the appearance changes of the samples containing 2% GO/Al_2O_3 nanoparticles, 2% nano-Al_2O_3, and control sample at 600 °C. Figure 8 indicates that the sample containing nano-GO/Al_2O_3 has less cracking and color change than the sample containing Al_2O_3 nanoparticles and the sample without nanoparticles.

According to Liu et al. [35], the change law of the damage degree of concrete specimen N10G2 was similar to that of specimen N10G1, while the damage degree of concrete appeared later and lighter than specimen N10G1. After 90 drying-wetting cycles, the damage degree of concrete specimen N10G2 was 0.157, and the squared correlation coefficient R2 after fitting was 0.97769. Compared with concrete specimen N10G1, the degree of damage was reduced by 22.47%. As a result, with the increase in the baking-immersing time ratio, the concrete damage and deterioration will further exacerbate.

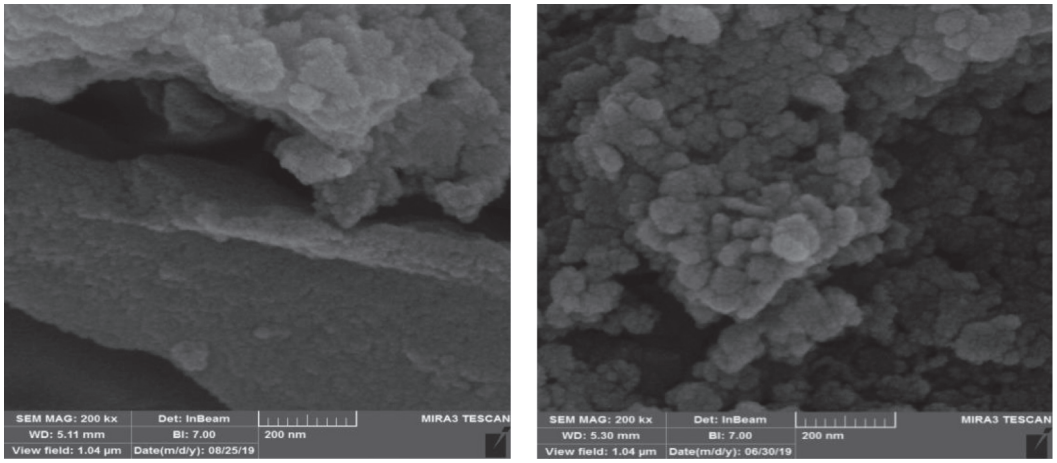

(a) (b)

Figure 5: SEM images of GO/Al_2O_3 NPs (a) and (b) Al_2O_3 NPs.

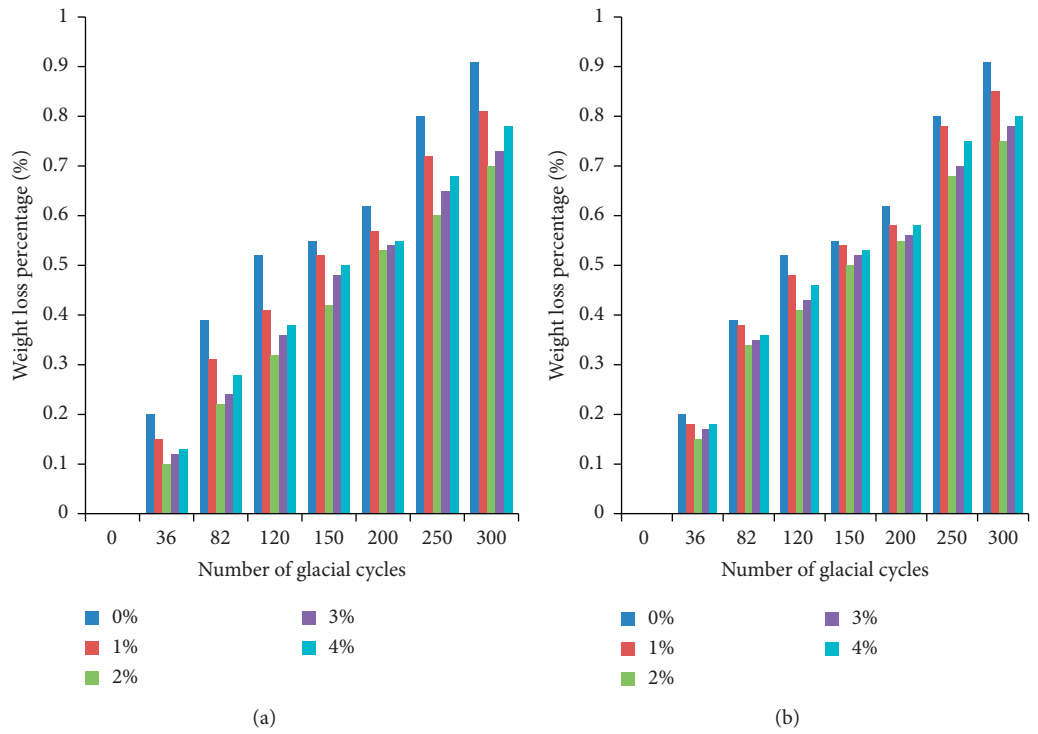

(a) (b)

Figure 6: Comparison of weight loss of the concrete samples containing (a) GO/Al_2O_3 nanoparticles and (b) Al_2O_3 nanoparticles.

3.2.3. Results of Weight Changes in Sulfuric Acid Solution. The test results of concrete weight changes in sulfuric acid solution were recorded, and the average percentage of relative changes of sample weights was determined in sulfuric acid solution.

Weight changes of samples proportional to the time of exposure to the sulfuric acid solution are shown in Figures 9 and 10. As can be observed, the weights increase in the first weeks due to acid reaction with calcium hydroxide to form gypsum.

Over time, the sulfuric acid solution dissolves the surface layer, and the sample weight is reduced by the destruction of this layer and leaching. As for the sample containing 2% GO/Al_2O_3 nanoparticles, the weight loss has been started after 12 weeks of placing in the sulfuric acid solution.

As shown in Figure 9, the samples containing 1% and 3% GO/Al_2O_3 nanoparticles showed higher weight loss. Samples containing 2% GO/Al_2O_3 nanoparticles have shown the best durability against sulfate attack. At the end of the 16^{th} week of placement in acid solution, about 1% of the weight of

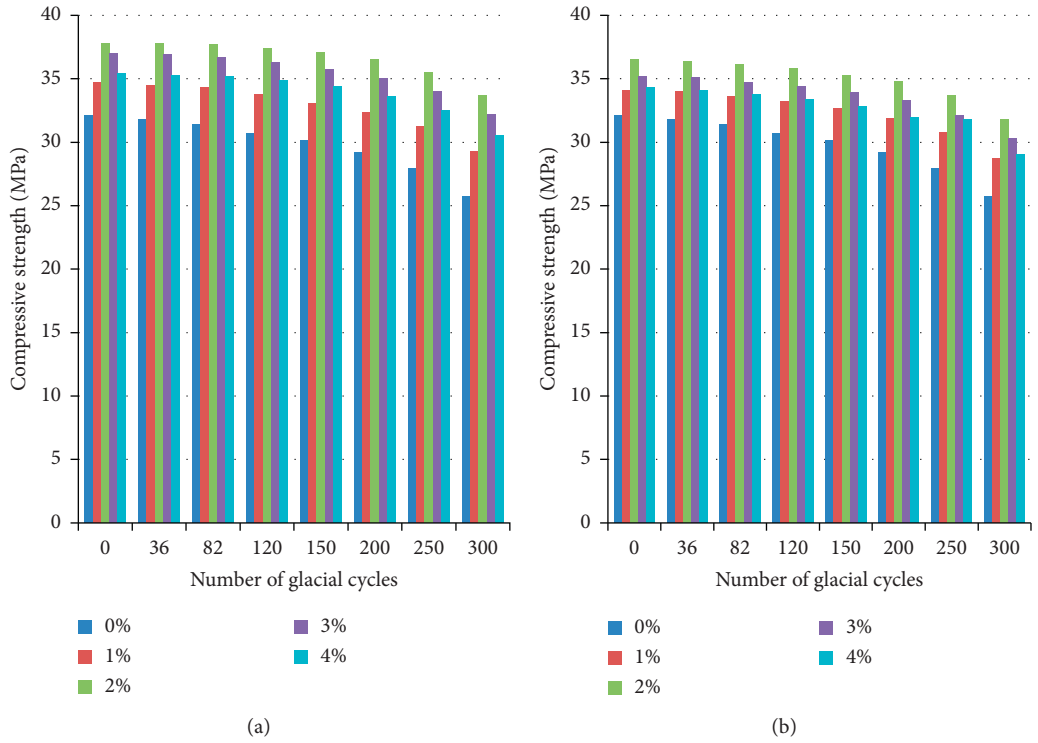

Figure 7: Compressive strength of samples under different freeze-thaw cycles: (a) GO/Al_2O_3 nanoparticles and (b) Al_2O_3 nanoparticles.

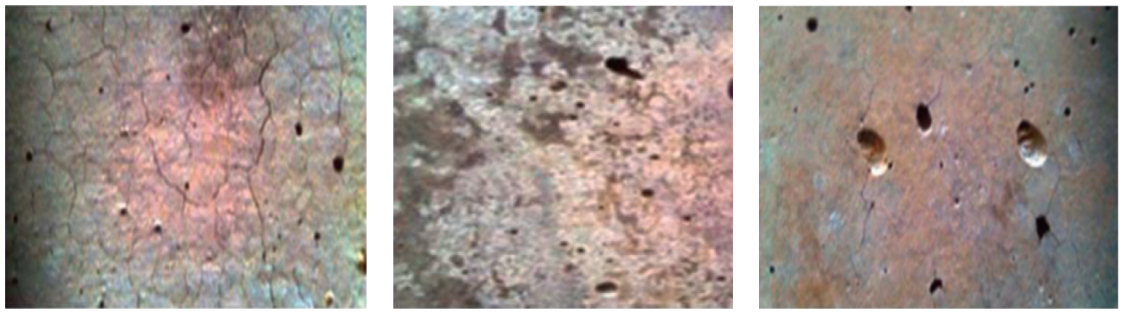

Figure 8: Concrete appearance changes at 600 ˚C: (a) control sample, (b) sample containing 2% Al_2O_3 nanoparticles, and (c) sample containing 2% GO/Al_2O_3 nanoparticles.

concrete was reduced, which was the least amount of weight loss among the samples.

The results of the placement of concrete containing Al_2O_3 nanoparticles in sulfuric acid (Figure 10) shows that the sample without nanoparticles and the samples containing 1% and 3% nano-Al_2O_3 had higher weight loss. Samples containing 2% of Al_2O_3 nanoparticles showed the best durability against the acidic condition, but the weight loss of Al_2O_3 nanoparticles was more than that of nano-GO/Al_2O_3.

3.2.4. Changes in Compressive Strength of Concrete Samples in Sulfuric Acid Solution. Three cubic specimens from each design were examined. The average testing results of each design at the age of 28 days (before immersion of the concrete specimens in sulfuric acid solution) are reported in Figure 11.

The compressive strength test was conducted on concrete samples in sulfuric acid solution after 4, 8, and 16 weeks, and the relative strength of the samples, compared to the 28-day compressive strength of the control sample, is shown in Figures 12 and 13. Figure 12 shows that only the samples containing 2% and 3% of GO/Al_2O_3 nanoparticles have increased compressive strength in the fourth week of placing the samples in solution. This was done by filling the holes of concrete with acid reaction products. In the eighth week, the compressive strength of the sample containing 2% GO/Al_2O_3 nanoparticles has increased while the other samples showed a reduction in compressive strength. At week 16, all samples had a higher compressive strength reduction than the sample containing 2% GO/Al_2O_3

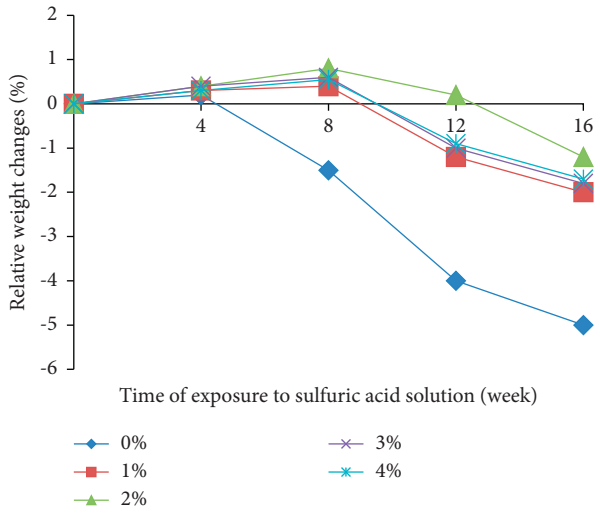

Figure 9: Relative weight changes of the concrete samples containing GO/Al_2O_3 nanoparticles in sulfuric acid.

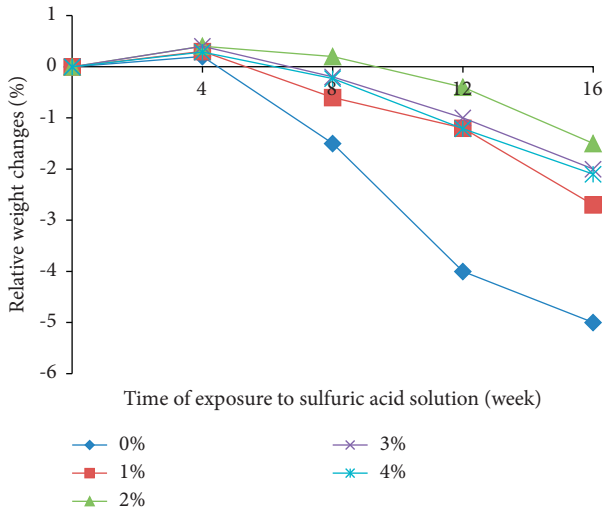

Figure 10: Relative weight changes of the concrete samples containing Al_2O_3 particles in sulfuric acid.

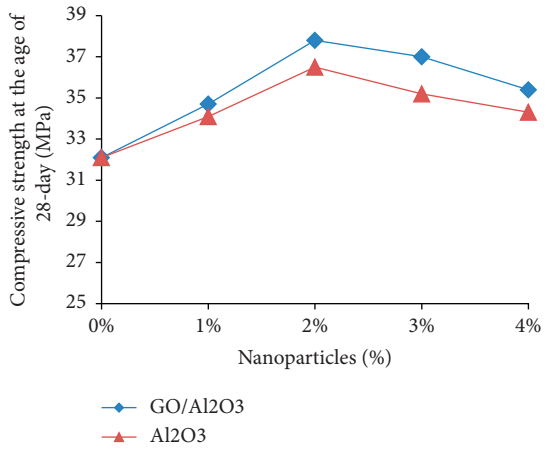

Figure 11: : Compressive strength of the concrete samples containing nanoparticles.

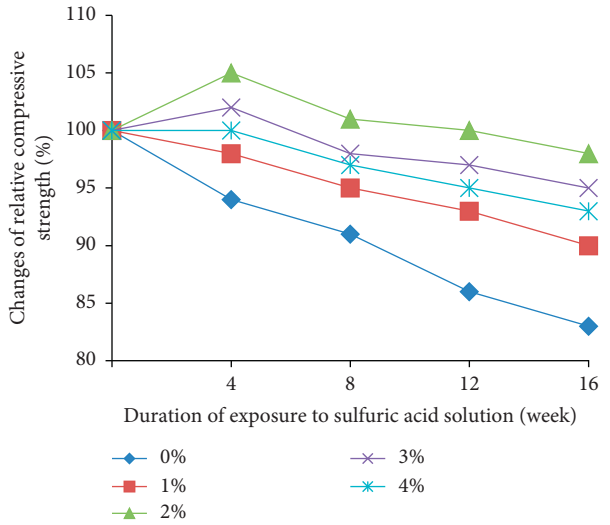

Figure 12: Changes in relative compressive strength of the concrete samples containing GO/Al_2O_3 particles in sulfuric acid.

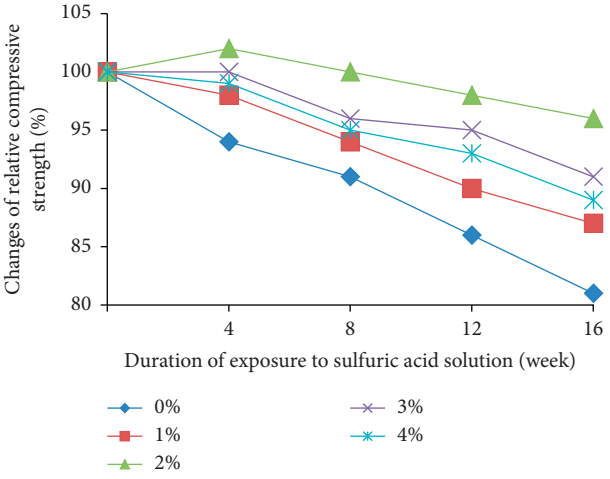

Figure 13: Changes in relative compressive strength of the concrete samples containing Al_2O_3 nanoparticles in sulfuric acid.

nanoparticles. The results confirm the sample containing 2% GO/Al_2O_3 nanoparticles as the optimum percentage.

The results of changes in relative compressive strength of the concrete samples containing Al_2O_3 nanoparticles in sulfuric acid solution were investigated. As shown in Figure 13, the samples containing 2% Al_2O_3 nanoparticles have increased compressive strength in the fourth week. However, this increase is lower than that of the samples containing GO/Al_2O_3. Therefore, the samples containing nano-GO/Al_2O_3 have better durability against acidic conditions.

3.3. Analysis of the Concrete Samples. After examining the durability of the samples and the best sample containing 2% nanoparticles, FT-IR, EDX, and SEM analyzes were conducted on the sample containing 2% nanoparticles, which confirm the use of nanoparticles as well as increased durability of concrete.

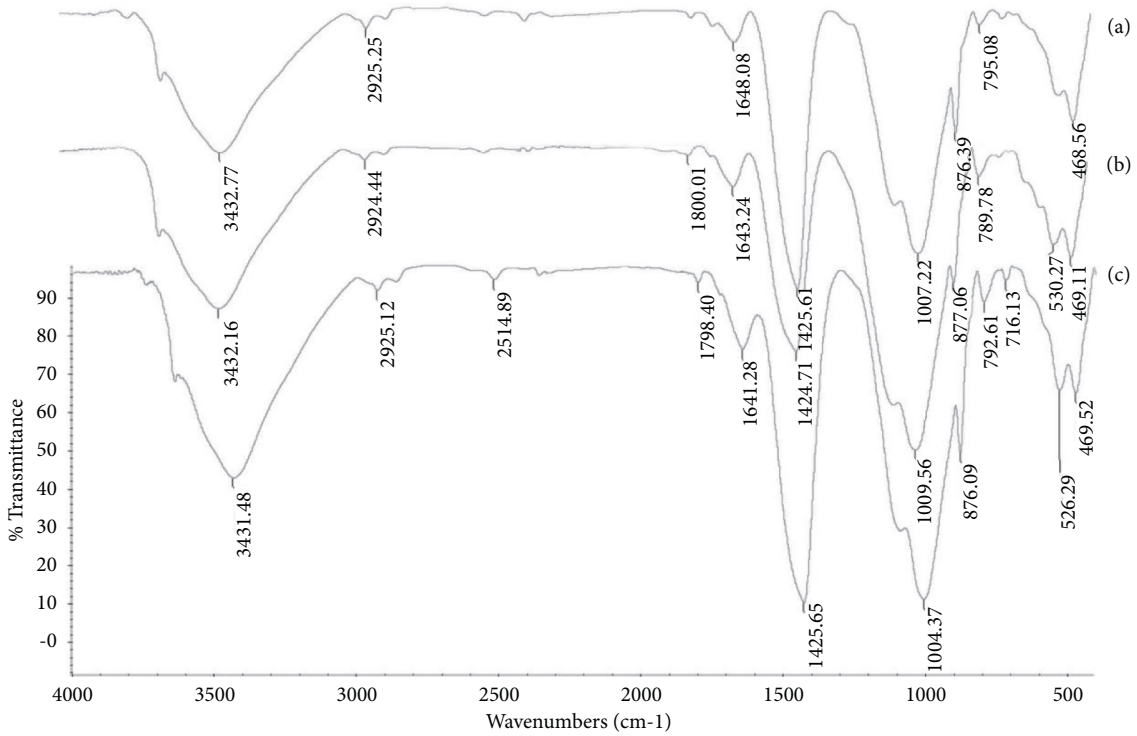

FIGURE 14: spectrum of (a) FT-IR of the control sample, (b) concrete containing 2% Al_2O_3 nanoparticles, and (c) concrete containing 2% GO/Al_2O_3 nanoparticles.

Infrared spectroscopy in Figure 14 shows similar transmission profiles for cementitious matrices. In the control sample, the stretches and vibrations of the OH and HOH chemical bonds, corresponding to the molecular and chemical bonded water in the wavelength, range between 3700 and 3200 cm^{-1} and about 11648 cm^{-1}, respectively. Carbonate bands in area 1425, hydrated calcium silicate in area 1007, and Al–O at 876 cm^{-1} were identified as the major constituents in Portland cement. Samples containing GO/Al_2O_3 and Al_2O_3 nanoparticles are calcium-silicate C-S-H hydrated peaks in the 1004–1010 region. The cause of this process is the large pores of calcium hydroxide $Ca(OH)_2$, transformed into smaller pores of C-S-H gel, thereby increasing the strength of the concrete.

To achieve an appropriate criterion for estimating the pozzolanic activity of the nanoparticles, X-ray diffraction experiments were performed on the powder obtained by grinding the cement paste samples in a nonnanoparticle mixing scheme with GO/Al_2O_3 and Al_2O_3 nanoparticles. The spectra obtained from the concrete containing nanoparticles were compared with the spectra of the control concrete sample. The samples were compared by their intensity after identifying the peaks related to calcium hydroxide.

In the pozzolanic reaction, large amounts of calcium hydroxide crystals are produced during the cement and water reaction. $Ca(OH)_2$ is a hexagonal crystal, located in the transition zone between the aggregates and the cement paste matrix, which is detrimental to concrete strengths.

Electron microscopy (SEM) images were taken for three cement paste schemes, including control plan, 2% GO/Al_2O_3 nanoparticles, and 2% Al_2O_3 nanoparticles, whose hydration reaction was stopped by acetone at 28 days of age.

As can be seen from the images of the hardened paste fracture surfaces, the presence of GO/Al_2O_3 and Al_2O_3 nanoparticles contributes to the density of the cement paste structure, and the concrete structure is clearly denser in the presence of these two materials. The appropriate form of density and uniformity of the concrete structure in the three samples at the age of 28 days shows that the difference between the density of the control sample and the other two samples is clear.

Comparison of the SEM images of the samples containing the nanoparticles in the figure shows that the GO/Al_2O_3 nanoparticles have a much greater effect on densifying the dough structure and removing its cavities at 28 days of age due to the more inactive GO/Al_2O_3 nanocrystals than the other samples (Figures 15(a)–15(c)).

Energy-dispersive X-ray spectroscopy (EDX) is an analytical method used for structural analysis or chemical properties of a sample. According to the foregoing, it is quite clear here that the amount of calcium in the sample containing GO/Al_2O_3 nanoparticles is much lower than in the control and Al_2O_3 samples (Figures 15(d)–15(f)).

With the continued progress of the hydration, the microstructure became more compact at 28 d. With the generation of new C-S-H gels and the growth of ettringite crystals, the internal pores in the cement became more completely filled. After 28 d, the C-S-H gels and ettringites attached to each other and needle-like ettringites were wrapped by the C-S-H gels, which also contributed to increasing the density [36].

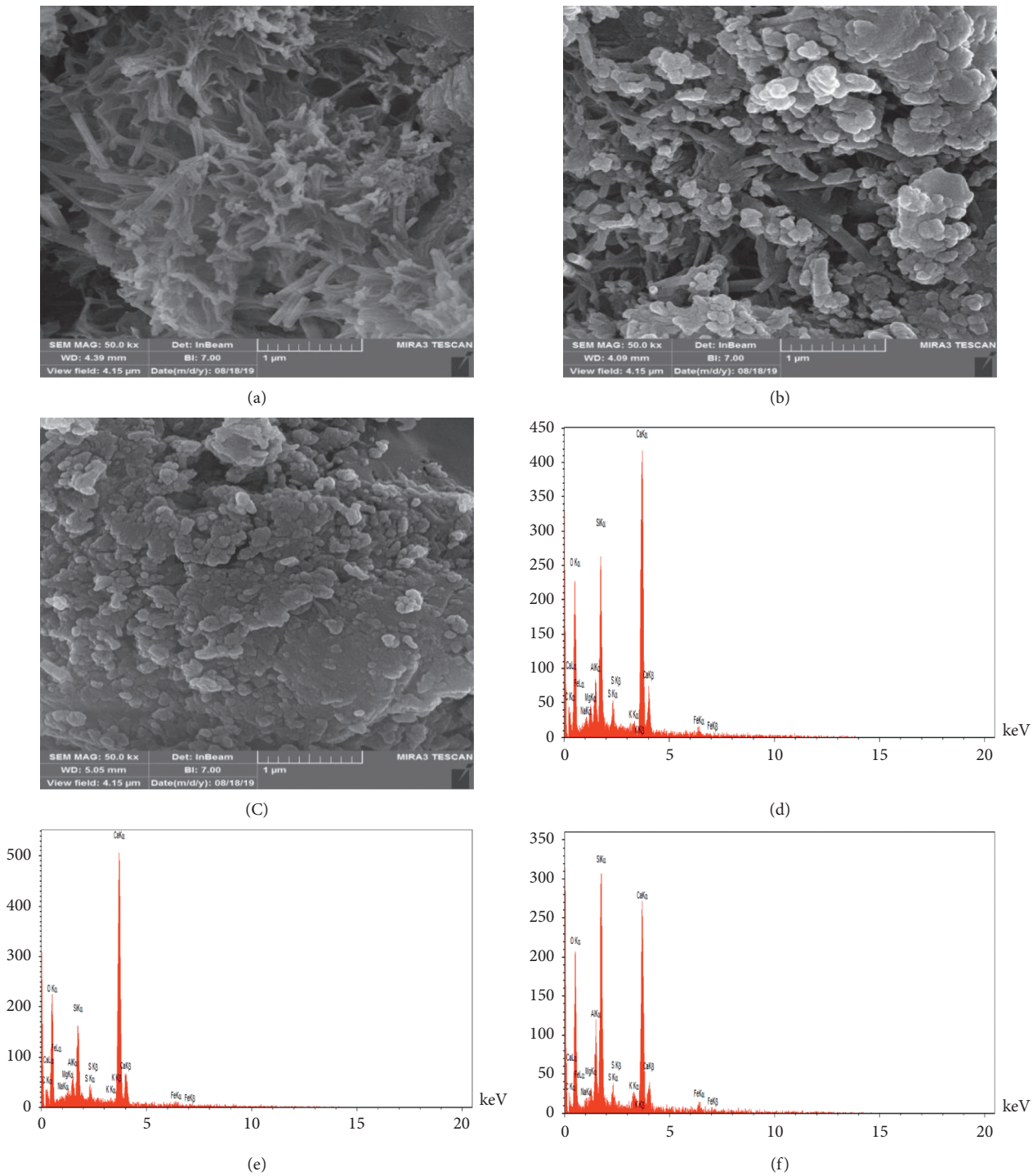

Figure 15: Spectrum of (a) SEM of the control sample, (b) concrete containing 2% Al_2O_3 nanoparticles, (C) concrete containing 2% GO/Al_2O_3 nanoparticles; (d) EDX of the control sample, (e) concrete containing 2% Al_2O_3 nanoparticles, and (f) concrete containing 2% GO/Al_2O_3 nanoparticles.

4. Conclusions

In this research, the effect of GO/Al_2O_3 nanoparticles was studied on the durability of concrete. The following results can be presented based on the laboratory work performed in this study.

By adding nanoparticles, the microstructure of concrete improves and the internal cavities of concrete reduces (the surface of samples containing nanomaterials becomes more uniform and dense), which improves the durability of concrete. Using nano-GO/Al_2O_3 causes a better durability against freeze-thaw cycle, sulfate attack, and high

temperature compared to nano-Al_2O_3. The proposed optimal composition for GO/Al_2O_3 and Al_2O_3 is 2% in this research. In general, 2% replacement of cement with GO/Al_2O_3 nanoparticles was appropriate in this study. The results of EDX, SEM, and FT-IR tests of concrete show that $Ca(OH)_2$ in the samples containing GO/Al_2O_3 nanoparticles decreases due to the reaction with nanoparticles, producing more hydrated calcium silicate (C-S-H gel), improves the microstructure of concrete, and subsequently, improves its properties.

Data Availability

The data used to support the findings of this study are included within the article.

Conflicts of Interest

The authors declare that they have no conflicts of interest.

References

[1] M. S. M. Norhasri, M. S. Hamidah, and A. M. Fadzil, "Applications of using nano material in concrete: a review," *Construction and Building Materials*, vol. 133, no. 15, pp. 91–97, 2017.

[2] P. Jaishankar, S. Kanchidurai, and K. Saravanarajamohan, "Durability and pore structure analysis of high performance concrete with nano silica," *Revista Română de Materiale/Romanian Journal of Materials*, vol. 50, no. 4, pp. 478–484, 2020.

[3] Y. Rahbar, S. Yasinmousavi, and H. Dashti Nasserabadi, "Performance of high-strength concrete made with binary and ternary blends of natural zeolite and nano-particles in aggressive environment," *Revista Română de Materiale/Romanian Journal of Materials*, vol. 50, no. 4, pp. 521–530, 2020.

[4] M. Lu, H. Xiao, M. Liu, X. Li, H. Li, and L. Sun, "Improved interfacial strength of SiO2 coated carbon fiber in cement matrix," *Cement and Concrete Composites*, vol. 91, pp. 21–28, 2018.

[5] M. Liu, H. Xiao, R. Liu, and J. Liu, "Dispersion characteristics of various contents of nano-TiO2 and its effect on the properties of cement-based composite," *Structural Concrete*, vol. 19, no. 5, pp. 1301–1308, 2018.

[6] G. Li, "Properties of high-volume fly ash concrete incorporating nano-SiO2," *Cement and Concrete Research*, vol. 34, no. 6, pp. 1043–1049, 2004.

[7] Y. L. Wang, Y. S. Wang, B. L. Wan, B. G. Han, G. C. Cai, and Z. Z. Li, "Properties and mechanisms of self-sensing carbon nanofibers/epoxy composites for structural health monitoring," *Composite Structures*, vol. 200, no. 15, pp. 669–678, 2018.

[8] E. Sadrossadat and H. Basarir, "An evolutionary-based prediction model of the 28-day compressive strength of high-performance concrete containing cementitious materials," *Advances in Civil Engineering Materials*, vol. 8, no. 3, pp. 484–497, 2019.

[9] A. Kooshkaki and H. Eskandari-Naddaf, "Effect of porosity on predicting compressive and flexural strength of cement mortar containing micro and nano-silica by multi-objective ANN modeling," *Construction and Building Materials*, vol. 212, no. 10, pp. 176–191, 2019.

[10] S. A. Emamian and H. Eskandari-Naddaf, "Genetic programming based formulation for compressive and flexural strength of cement mortar containing nano and micro silica after freeze and thaw cycles," *Construction and Building Materials*, vol. 241, no. 30, Article ID 118027, 2020.

[11] G. Quercia, G. Hüsken, and H. J. H. Brouwers, "Water demand of amorphous nano silica and its impact on the workability of cement paste," *Cement and Concrete Research*, vol. 42, no. 2, pp. 344–357, 2012.

[12] Y. Wang, G. Chen, B. Wan, H. Lin, and J. Zhang, "Behavior of innovative circular ice filled steel tubular stub columns under axial compression," *Construction and Building Materials*, vol. 171, no. 20, pp. 680–689, 2018.

[13] S. Zhutovsky and K. Kovler, "Effect of internal curing on durability-related properties of high performance concrete," *Cement and Concrete Research*, vol. 42, no. 1, pp. 20–26, 2012.

[14] Y. Zhang, C. Liu, Z. Liu, G. Liu, and L. Yang, "Modelling of diffusion behavior of ions in low-density and high-density calcium silicate hydrate," *Construction and Building Materials*, vol. 155, no. 30, pp. 965–980, 2017.

[15] J. Sorathiya, S. Shah, and S. Kacha, "Effect on addition of nano "titanium dioxide" (TiO_2) on compressive strength of cementitious concrete," *Kalpa Publications in Civil Engineering*, vol. 1, pp. 219–225, 2017.

[16] Y. Zhang and X. Kong, "Influences of superplasticizer, polymer latexes and asphalt emulsions on the pore structure and impermeability of hardened cementitious materials," *Construction and Building Materials*, vol. 53, no. 28, pp. 392–402, 2014.

[17] E. Güneyisi, M. Gesoğlu, E. Booya, and K. Mermerdas, "Strength and permeability properties of self-compacting concrete with cold bonded fly ash lightweight aggregate," *Construction and Building Materials*, vol. 74, no. 15, pp. 17–24, 2015.

[18] B.-W. Jo, C.-H. Kim, G.-h. Tae, and J.-B. Park, "Characteristics of cement mortar with nano-SiO2 particles," *Construction and Building Materials*, vol. 21, no. 6, pp. 1351–1355, 2007.

[19] A. H. Shekari and M. S. Razzaghi, "Influence of nano particles on durability and mechanical properties of high performance concrete," *Procedia Engineering*, vol. 14, pp. 3036–3041, 2011.

[20] J. Kim, L. J. Cote, F. Kim, W. Yuan, K. R. Shull, and J. Huang, "Graphene oxide sheets at interfaces," *Journal of the American Chemical Society*, vol. 132, no. 23, pp. 8180–8186, 2010.

[21] A. P. Singh, M. Mishra, A. Chandra, and S. K. Dhawan, "Graphene oxide/ferrofluid/cement composites for electromagnetic interference shielding application," *Nanotechnology*, vol. 22, no. 46, Article ID 465701, 2011.

[22] Z. Xu and C. Gao, "Aqueous liquid crystals of graphene oxide," *ACS Nano*, vol. 5, no. 4, pp. 2908–2915, 2011.

[23] L. Li, Y. Pan, T. Wu, and H. Bao, "Green fabrication of chitosan films reinforced with parallel aligned graphene gxide," *Carbohydrate Polymers*, vol. 83, no. 4, pp. 1908–1915, 2011.

[24] Q. Ma and Y. Zhu, "Experimental research on the microstructure and compressive and tensile properties of nano-SiO 2 concrete containing basalt fibers," *Underground Space*, vol. 2, no. 3, pp. 175–181, 2017.

[25] P. Zhang, K. Wang, J. Wang, J. Guo, S. Hu, and Y. Ling, "Mechanical properties and prediction of fracture parameters of geopolymer/alkali-activated mortar modified with PVA fiber and nano-SiO2," *Ceramics International*, vol. 46, no. 12, pp. 20027–20037, 2020.

[26] L. Wang, F. Guo, Y. Lin, H. Yang, and S. W. Tang, "Comparison between the effects of phosphorous slag and fly ash on the C-S-H structure, long-term hydration heat and volume

deformation of cement-based materials," *Construction and Building Materials*, vol. 250, no. 2, 2020.
[27] W. S. Hummers and R. E. Offeman, "Preparation of graphitic oxide," *Journal of the American Chemical Society*, vol. 80, no. 6, p. 1339, 1958.
[28] Astm Standard C33, *Specification for Concrete Aggregates*, ASTM International, West Conshohocken, PA, 2003.
[29] Aci 318-83, *Building Code Requirements for Rein Forceced concrete*, American Conerete Insrtit, Michigan, 1983.
[30] Bs 1881, *Testing Concrete. Method for Determination of Compressive Strength of Concrete Cubes*, BSI, London, 1983.
[31] Astm C666-97, *Standard Test Method for Resistance of Concrete to Rapid Freezing and Thawing*, ASTM International, West Conshohocken, PA, 1997.
[32] Astm C1012, *Length Change of Hydraulic-Cement Mortars Exposed to a Sulfate Solution*, ASTM International, West Conshohocken, PA, 2004.
[33] I. Hager, "Behaviour of cement concrete at high temperature," *Bulletin of the Polish Academy of Sciences, Technical Sciences*, vol. 61, no. 1, pp. 145–154, 2013.
[34] M. Acik, G. Lee, C. Mattevi et al., "The role of oxygen during thermal reduction of graphene oxide studied by infrared absorption spectroscopy," *Journal of Physical Chemistry C*, vol. 115, no. 40, pp. 19761–19781, 2011.
[35] F. Liu, Z. You, R. Xiong, and X. Yang, "Effects of sodium sulfate attack on concrete incorporated with drying-wetting cycles," *Advances in Civil Engineering*, vol. 2021, Article ID 5393504, 12 pages, 2021.
[36] Y. Sun, P. Zhang, W. Guo, J. Bao, and C. Qu, "Effect of nano-CaCO3 on the mechanical properties and durability of concrete incorporating fly ash," *Advances in Materials Science and Engineering*, vol. 2020, Article ID 7365862, 10 pages, 2020.